Remote Sensing of Environment 230 (2019) 111190

Contents lists available at ScienceDirect

Remote Sensing of Environment

journal homepage: www.elsevier.com/locate/rse

Developing a common globally applicable method for optical remote sensing of ecosystem light use efficiency

Karl F. Huemmrich[a,*], Petya Campbell[a], David Landis[b], Elizabeth Middleton[c]

[a] University of Maryland Baltimore County, Code 618, Goddard Space Flight Center, Greenbelt, MD 20771, USA
[b] Global Science and Technology Inc. Greenbelt, MD, USA
[c] National Aeronautics and Space Administration, Goddard Space Flight Center, Greenbelt, MD, USA

ARTICLE INFO

Edited by Jing M. Chen

Keywords:
Earth observing 1
Hyperion
Light use efficiency
Terrestrial ecosystem productivity
Hyperspectral imaging

ABSTRACT

This study examines the use of spectral reflectance to determine ecosystem photosynthetic light use efficiency (LUE) during mid-growing season for 32 globally distributed flux tower sites. Surface reflectance for 133 spectral bands were extracted for areas around the flux towers from imagery collected by the Hyperion instrument on the Earth Observing 1 satellite. The average reflectance spectra were matched with LUE derived from CO_2 flux data collected using eddy covariance techniques from the La Thuile Fluxnet Synthesis Dataset, resulting in 79 observations collected between 2000 and 2007. LUE was calculated from daily gross ecosystem production (GEP) and incident photosynthetically active radiation (PAR) from the flux towers and MODIS fraction of absorbed PAR (fPAR). An examination of all possible two band normalized difference vegetation indices found that no index performed better than R^2 of 0.55, although 60 of the bands were included in normalized difference indices with a $R^2 > 0.45$. A partial least squares regression (PLSR) using all spectral bands produced a R^2 of 0.81, suggesting the use of this approach to develop a globally-applicable retrieval method for LUE using spectral imagery from future missions flying imaging spectrometers, such as the NASA Surface Biology and Geology mission.

1. Introduction

Ecosystems have varying capacities for photosynthetic carbon uptake and also vary in their responses to environmental conditions. These fundamental characteristics of the biospheric metabolism are spatially and temporally variable and are affected by ongoing changes in atmospheric CO_2 composition, climate, land use, and other stressors (Schimel et al., 2015; Ciais et al., 2014). Under changing climate and disturbance regimes it is important to understand the nature of these variations and how they affect terrestrial ecosystem carbon fluxes (Michalak et al., 2011) because these responses define the nature and magnitude of climatic feedbacks (Piao et al., 2013; Friend et al., 2014; Hoffman et al., 2014) resulting in a need for descriptions of regional and global patterns of ecosystem productivity.

Ground measurements using eddy covariance techniques provide descriptions of temporal changes in ecosystem carbon uptake at flux tower sites (Baldocchi, 2008). However, ecosystem/atmosphere models must be used to describe fluxes in areas beyond the tower sites (Ciais et al., 2014). Remotely sensed data may be used to provide spatially explicit inputs for these models (Schimel et al., 2015; Ciais et al., 2014). The difficulties in accurately describing photosynthetic responses to environmental stresses (e.g., nutrient, moisture, temperature or vapor pressure deficit) cause uncertainties in estimates made by ecosystem/atmosphere carbon exchange models. Not only are these dynamic effects difficult to model, but also some model inputs (e.g., root zone soil moisture) are not available at the required spatial and temporal scales (Schaefer et al., 2012).

One approach for modeling gross ecosystem production (GEP) is the light use efficiency (LUE) model. At its simplest, LUE models have the form:

$$G = \varepsilon f\mathrm{APAR}\ \mathrm{Qin} = \varepsilon\ \mathrm{APAR}. \quad (1)$$

Which can be rearranged to give:

$$\varepsilon = G/\mathrm{APAR} \quad (2)$$

where, G is gross ecosystem production (GEP), Qin is the incoming photosynthetically active radiation (PAR), *f*APAR is the fraction of PAR absorbed by vegetation, APAR is the PAR absorbed by vegetation or the product of *f*APAR and Qin, and ε is the LUE which can be expressed in units of mol carbon mol^{-1} absorbed photons (Monteith, 1977; Russell

* Corresponding author.
E-mail address: karl.f.huemmrich@nasa.gov (K.F. Huemmrich).

https://doi.org/10.1016/j.rse.2019.05.009
Received 26 July 2018; Received in revised form 12 February 2019; Accepted 9 May 2019
Available online 22 May 2019

et al., 1989).

In LUE models, such as the MODIS Gross Primary Production model (the MOD017 Product) (Running and Zhao, 2015; Running et al., 2004) and the CASA model (Potter et al., 1993) *f*APAR is determined using remote sensing observations while LUE (ε) is calculated based on an assumed maximum unstressed LUE, defined by vegetation class, which is then scaled down using functions driven by environmental variables such as air temperature and vapor pressure deficit. Comparisons of the MOD17 output with ground measured GEP for forest sites found differences in the LUE (Turner et al., 2003), while at other sites the maximum LUE parameter used by the MODIS algorithm was much higher than those calculated using ground-based flux tower measurements (Martel et al., 2005). These kinds of uncertainties in the determination of LUE affect differences among models, with the parameterization of LUE calculations being a large source of model uncertainty (Jung et al., 2007; Lin et al., 2011).

An alternative to modeling LUE is to directly infer its value based on remotely sensed optical signals. One method is a multispectral approach using spectral vegetation indices (SVI), which are algebraic combinations of reflectances from several spectral bands. One approach using SVI to remotely sense LUE or GEP estimates chlorophyll content (Dawson et al., 2003; Houborg et al., 2011; Kergoat et al., 2008; Peng and Gitelson, 2011, and Peng et al., 2011). Another method uses the Photochemical Reflectance Index (PRI), a SVI indicator of stress responses related to changes in the xanthophyll cycle pigments and/or changes in the ratio of chlorophyll to carotenoid pigment concentrations (Grace et al., 2007; Hilker et al., 2008; Coops et al., 2010; Garbulsky et al., 2011; Peñuelas et al., 2011; Middleton et al., 2011, 2016; Gamon et al., 2016).

LUE variability over a landscape has also been derived from descriptions of the distribution of plant functional types, having different LUE, determined from spectral unmixing (Huemmrich et al., 2013). Other studies have made use of information in the full spectrum or selected spectral regions to obtain spectral derivatives or band depths for absorption features using continuum removal to derive GEP (Campbell et al., 2013; Huemmrich et al., 2017). Yet another approach estimates Vcmax, the maximum velocity of RuBP carboxylation, a key parameter describing photosynthesis, using a partial least squares regression (PLSR) approach over the entire reflectance spectrum of leaves and canopies (Serbin et al., 2011, 2015). All of these types of studies demonstrate how information derived from spectral reflectance can describe vegetation characteristics related to GEP. However, these studies have been limited to a few sites and generally suggest that relationships between SVI and LUE differ among different vegetation types, thus complicating their use in regional or global studies.

Any attempt to use optical approaches to estimate LUE globally must therefore address the issue of possible differences in responses of SVI in different vegetation types. Ideally, when used as a metric for some variable, in this case LUE, a SVI should have three characteristics: 1) it should be related to the variable of interest, 2) it should be insensitive to other characteristics of the scene, and 3) for ease of scaling and interpretation, it should have a linear relationship with the variable of interest. The second characteristic may be particularly problematic in the development of globally-applied algorithms. A variety of landscape, view, and illumination factors may affect vegetation indices, such as background reflectance, variations in leaf angle and leaf optical properties, presence of non-green material in the canopy, and canopy shadowing (Goward and Huemmrich, 1992; Barton and North, 2001; Huemmrich and Goward, 1997).

One solution to managing these secondary effects is to use a land cover classification as a first step to decide the algorithm/coefficients to be used in the retrieval of LUE. There is precedence for this approach as it is used in some global MODIS products, such as for leaf area index and gross primary production (Lotsch et al., 2003). However, the accuracy of MODIS land cover types is estimated to be no better than 60–80% overall, such that 20–40% of the pixels are mis-classified (Friedl et al., 2010; Herold et al., 2008). Retrievals from mis-classified pixels can result in significant errors (Fang et al., 2013). The interpretation of results is further complicated for mixed pixels, those having multiple cover types. An ideal algorithm would therefore be insensitive to variations in vegetation types to avoid this problem.

This study examines different approaches with the aim of a single algorithm driven by spectral reflectance to provide an estimate of LUE over a wide range of vegetation types that can meet the three criteria described above by accounting for variability among sites yet still providing a linear relationship between a metric and LUE.

This would represent an important improvement in the use of optical data to map GEP, both locally and globally, from imaging spectrometers such as in the planned NASA Surface Biology and Geology (SBG) mission. To develop such an algorithm requires a consistent set of both hyperspectral reflectance and ecosystem CO_2 flux measurements. This study is possible due to the collection of globally distributed imagery from the Hyperion imager on the Earth Observing 1 (EO-1) satellite combined with eddy covariance flux measurements consistently processed in the Fluxnet Synthesis Dataset and the existing MODIS *f*APAR product. The aim of this study is to explore an approach that may be applied to future satellite hyperspectral imagery, such as from SBG, to derive algorithms for describing biophysical characteristics over widely varying ecosystems. Here we focus on variability in LUE across different sites rather than seasonal variability (e.g. Campbell et al., 2013). This is one of the first studies to examine a large number of widely distributed sites using Hyperion imagery in a cross-site analysis. Due to the number and separation of sites the collection of spectral reflectance imagery for this type of study would be logistically difficult and expensive to perform using aircraft mounted imaging spectrometers.

We consider two approaches to estimate LUE from optical data: a multispectral approach that uses SVI and a hyperspectral approach using PLSR to examine methods that may accommodate variability in vegetation structure and responses to produce a consistent output. This analysis could be considered as a scenario where hyperspectral data are used to derive LUE in support of the existing MODIS GEP product, either by directly determining LUE for the model or providing LUE in a data assimilation approach.

2. Methods

EO-1 is an important platform for global studies, as the same spectrometer imaged globally-distributed sites over an extended time period. Hyperion imagery have 30 m spatial resolution, typically imaging 7 km x ~100 km scenes, with spectra having approximately 10 nm spectral resolution ranging from 400 to 2500 nm. EO-1 was launched in 2000 and collected over 34,000 globally-distributed Hyperion images through 2007 and over 90,000 total images over the mission lifetime (Middleton et al., 2013). Based on a time series of observations of stable surface targets, Hyperion has been shown to be radiometrically stable over its lifetime showing little drift in radiance measurements (Campbell et al., 2013). Previous work has shown relationships between Hyperion spectral reflectances and carbon flux variables for a limited number of sites (Campbell et al., 2013; Huemmrich et al., 2013). The Hyperion images were retrieved using Earth Explorer, courtesy of the NASA EOSDIS Land Processes Distributed Active Archive Center (LP DAAC), USGS/Earth Resources Observation and Science (EROS) Center, Sioux Falls, South Dakota, https://earthexplorer.usgs.gov/.

Hyperion imagery were atmospherically corrected to surface reflectance using the ATmosphere REMoval algorithm (ATREM) (Gao and Davis, 1997; Gao et al., 2009). ATREM uses the 6S radiative transfer model (Kotchenova et al., 2006) to account for the changes in solar illumination, and explicitly simulate the absorption and scattering effects of atmospheric gases and aerosols. Due to atmospheric effects and instrument problems, only 133 out of 220 Hyperion spectral bands were

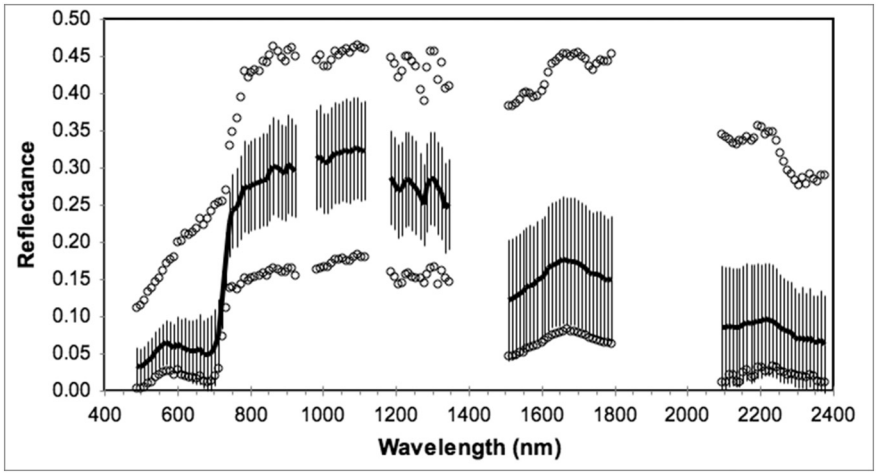

Fig. 1. Spectral reflectance of usable Hyperion bands, the black line is the mean reflectance for all observations, with error bars ± 1 standard deviation and the open circles are the maximum and minimum values for each band.

found to be usable (Fig. 1).

The Hyperion images were matched up with CO_2 flux data that were collected using eddy covariance techniques and compiled in the La Thuile Fluxnet Synthesis Dataset (data available at http://www.fluxdata.org) (Agarwal et al., 2010). The La Thuile Fluxnet Synthesis Dataset contains data from 253 different flux towers that have been processed in a consistent manner (Papale et al., 2006; Reichstein et al., 2005; Moffat et al., 2007). The flux data were matched with the available Hyperion imagery to identify cases with clear images collected over operating flux towers during the local growing season from 2001 to 2007.

To capture the growing season, the imagery in this study were collected between May and September for sites north of 30°N, while for tropical sites images were collected as late as November, with a December image included for the Australian site in the southern hemisphere. The focus of this study was to attempt to detect how biochemical changes in plants may provide information on LUE, so the imagery used were constrained to periods with small seasonal changes in MODIS derived *f*APAR (Gamon, 2015). The selection process identified 32 flux tower sites with usable data. These sites were globally distributed, although most were located in North America (Table 1, Fig. 2). The sites included a number of vegetation types: evergreen needleleaf forests, evergreen broadleaf forests, croplands, and deciduous forests comprised most of the vegetation types (Fig. 3a). There were a total of 79 usable Hyperion images (Fig. 3b, Table 1).

GEP values in the Fluxnet Synthesis Dataset were determined from eddy covariance measurements which were filtered, despiked, gap filled, and had the net ecosystem exchange partitioned into GEP and ecosystem respiration following standard algorithms (Papale et al., 2006; Reichstein et al., 2005). Flux data values were provided as half hour averages.

Daily LUE was calculated following Eq. (2) using integrated daily G and Qin for day of the imagery. MODIS *f*APAR values for the image day were estimated using a linear interpolation of high quality 8-day values (data available from Oak Ridge DAAC https://modis.ornl.gov/cgi-bin/MODIS/global/subset.pl). MODIS *f*APAR values were used as an independent and globally consistent product (Xu et al., 2018). The sites represent a range in physical structure, indicated by *f*APAR which varied between 0.13 and 0.95, and in photosynthetic efficiency with daily LUE values ranging between 0.00076 and 0.0473 mol CO_2 mol^{-1} absorbed photons. LUE uncertainties were estimated assuming a 15% uncertainty in GEP (Schmidt et al., 2012, Raj et al., 2016), a constant 0.1 *f*APAR (Xu et al., 2018), and 2% in incident PAR (Schmidt et al., 2012). The spatial mismatches among the flux tower footprints, the extracted Hyperion pixels, and the 1 km MODIS pixels are a further source of noise that have not been quantified in this analysis.

For this analysis spectra were extracted from the Hyperion imagery for pixels representing relatively uniform areas around each flux tower and were averaged to improve signal to noise ratio. The number of pixels extracted from around the tower sites varied, based on a visual inspection of the image to describe the largest reasonable contiguous area of uniform vegetation coverage around the tower. The size of the selected areas varied between sixteen 30 m pixels, in heterogeneous logged or agriculture areas, to 196 pixels, in extensively forested areas (or 4 × 4 to 14 × 14 pixels).

LUE based on the half-hourly flux values at the Hyperion overpass time were also calculated. In the analyses these half-hourly values showed similar results to daily LUE, so only the daily LUE results are reported here.

2.1. Analysis approaches

This study examined SVI of every combination of two band normalized difference vegetation indices. We also evaluated first derivatives of the reflectance spectrum calculated using a 5-point linear Savitzky–Golay filter (Savitzky and Golay, 1964).

The second approach relating reflectance spectra to LUE used an empirical partial least squares regression (PLSR). Rather than making use of only two or three spectral bands, as the SVI do, PLSR utilizes information from all of the available spectral bands in an approach that maximizes covariance between the independent and dependent variables, while keeping factors derived from the input spectral data orthogonal (Wold et al., 2001). PLSR was developed to address problems where there are relatively few samples with many predictor variables, which may also be correlated (Boulesteix and Strimmer, 2006). PLSR was developed for chemical analysis spectroscopy and recently has been used in analysis of remotely sensed spectroscopy (e.g. Asner et al., 2015; Serbin et al., 2011, 2015; Martin et al., 2008; Huemmrich et al., 2017). A PLSR model was developed using the R package pls (Mevik and Wehren, 2007) applied to 133 Hyperion bands to derive LUE. The model was developed by using random cross validations for 100 repetitions of 39 sample subsets.

Performance of all of the different approaches was evaluated using the coefficient of determination (R^2) and standard error of regression for linear regressions.

3. Results

Simpler than a SVI are the individual band reflectances, and Fig. 1 shows the spectral shape along with the variability within each spectral

Table 1
Study site descriptions. Codes for landcover types are: EBF, Evergreen Broadleaf Forest; MF, Mixed Forest; WET, Wetlands; ENF, Evergreen Needleleaf Forest; DBF, Deciduous Broadleaf Forest; CRO, Cropland; GRA, Grassland; WSA, Woody Savanna; CSH, Closed Shrubs.

Site ID	Site name	Country	Latitude	Longitude	Landcover type	Hyperion obs. dates (year/day of year)
AU-Tum	Tumbarumba (Leuning et al., 2005)	Australia	−35.6557	148.1520	EBF	2001/347
BR-Cax	Caxiuana Forest-Almeirim (Baker et al., 2004, Carswell et al., 2002, Sommer et al., 2002)	Brazil	−1.7197	−51.4590	EBF	2002/248
BR-Ma2	Manaus - ZF2 K34 (Araújo et al., 2002)	Brazil	−2.6091	−60.2093	EBF	2002/226, 2005/218
BR-Sa1	Santarem-Km67-Primary Forest (Rice et al., 2004)	Brazil	−2.8567	−54.9589	EBF	2002/189, 2002/262, 2002/269, 2002/285
BR-Sa3	Santarem-Km83-Logged Forest (Da Rocha et al., 2004, Vourlitis et al., 2004)	Brazil	−3.0180	−54.9714	EBF	2002/189, 2002/262, 2002/269, 2002/285, 2003/185, 2003/217, 2003/233
CA-Ca1	British Columbia- Campbell River - Mature Forest Site (Humphreys et al., 2003, 2006)	Canada	49.8672	−125.3340	ENF	2005/207, 2005/223
CA-Ca2	British Columbia- Campbell River - Clearcut Site (Humphreys et al., 2006)	Canada	49.8705	−125.2910	ENF	2005/207, 2005/223
CA-Ca3	British Columbia- Campbell River - Young Plantation Site (Humphreys et al., 2006)	Canada	49.5346	−124.9000	ENF	2004/246
CA-Gro	Ontario- Groundhog River-Mat. Boreal Mixedwood (McCaughey et al., 2006)	Canada	48.2167	−82.1556	MF	2005/196
CA-Mer	Eastern Peatland- Mer Bleue (Lafleur et al., 2003)	Canada	45.4094	−75.5186	WET	2004/159
CA-NS1	UCI-1850 burn site (Goulden et al., 2006)	Canada	55.8792	−98.4839	ENF	2004/189, 2004/205
CA-NS2	UCI-1930 burn site (Bond-Lamberty et al., 2004, Goulden et al., 2006)	Canada	55.9058	−98.5247	ENF	2001/212
CA-NS5	UCI-1981 burn site (Bond-Lamberty et al., 2004, Goulden et al., 2006)	Canada	55.8631	−98.4850	ENF	2004/189, 2004/205
CA-Ojp	Sask.- SSA Old Jack Pine (Baldocchi et al., 1997)	Canada	53.9163	−104.6920	ENF	2002/236
CA-SJ1	Sask.- 1994 Harv. Jack Pine (Coursolle et al., 2006)	Canada	53.9080	−104.6560	ENF	2001/192, 2001/224, 2002/211, 2002/236
CN-Hny	Hunan Yueyang	China	29.3100	112.5100	DBF	2005/196
FR-Pue	Puechabon (Rambal et al., 2004)	France	43.7414	3.5958	EBF	2004/170, 2004/186
IE-Ca1	Carlow1 (Gilmanov et al., 2007)	Ireland	52.8588	−6.9181	CRO	2004/137
US-Bar	NH - Bartlett Experimental Forest (Ouimette et al., 2018)	USA	44.0646	−71.2881	DBF	2005/204, 2005/220
US-Bkg	SD – Brookings (Gilmanov et al., 2005, Schmidt et al., 2011)	USA	44.3453	−96.8362	GRA	2004/273, 2006/123, 2006/143
US-Ha1	MA - Harvard Forest EMS Tower (HFR1) (Urbanski et al., 2007)	USA	42.5378	−72.1715	DBF	2001/248, 2002/251, 2002/260
US-Ho1	ME - Howland Forest (main tower) (Hollinger et al., 1999)	USA	45.2041	−68.7402	ENF	2001/202, 2001/234, 2001/250, 2001/266, 2002/237, 2002/244, 2003/201, 2003/240, 2003/249
US-Ho2	ME - Howland Forest (west tower) (Davidson et al., 2006)	USA	45.2091	−68.7470	ENF	2001/202, 2001/234, 2001/250, 2001/266, 2002/237, 2002/244, 2003/201, 2003/240
US-Ivo	AK – Ivotuk (McEwing et al., 2015)	USA	68.4865	−155.7500	WET	2005/227
US-KS1	FL - Kennedy Space Center (slash pine) (Bracho et al., 2008)	USA	28.4583	−80.6709	ENF	2002/160
US-KS2	FL - Kennedy Space Center (scrub oak) (Powell et al., 2006)	USA	28.6086	−80.6715	CSH	2002/160
US-LPH	MA - Little Prospect Hill (Magill et al., 2004)	USA	42.5419	−72.1850	DBF	2002/251, 2002/260
US-Ne1	NE - Mead - irrigated continuous maize site (Verma et al., 2005, Suyker et al., 2004, 2005)	USA	41.1651	−96.4766	CRO	2005/124
US-Ne2	NE - Mead - irrigated maize-soybean rotation site (Verma et al., 2005, Suyker et al., 2004, 2005)	USA	41.1649	−96.4701	CRO	2001/225, 2001/241, 2005/124
US-Ne3	NE - Mead - rainfed maize-soybean rotation site (Verma et al., 2005, Suyker et al., 2004, 2005)	USA	41.1797	−96.4397	CRO	2001/225, 2001/241
US-SP3	FL - Slashpine-Donaldson-mid-rot- 12 yrs. (Clark et al., 1999, 2004)	USA	29.7548	−82.1633	ENF	2002/295, 2002/318
US-SRM	AZ - Santa Rita Mesquite (Scott et al., 2009)	USA	31.8214	−110.8660	WSA	2005/260, 2006/134, 2006/139, 2006/144, 2006/149

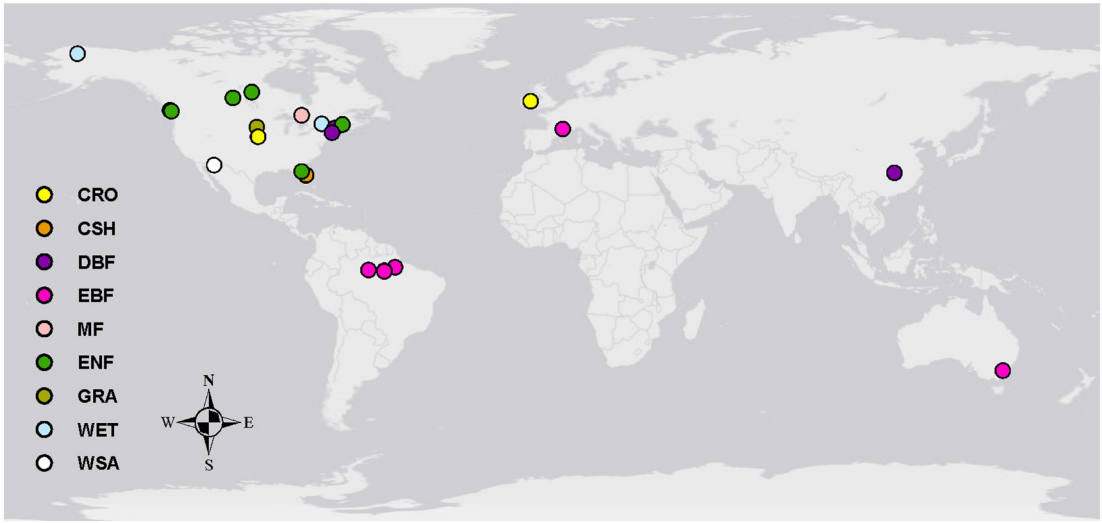

Fig. 2. Locations of sites used in this study. The color of the points indicates the vegetation type. The codes for vegetation types in the legend are provided in caption for Table 1. There are 32 different sites.

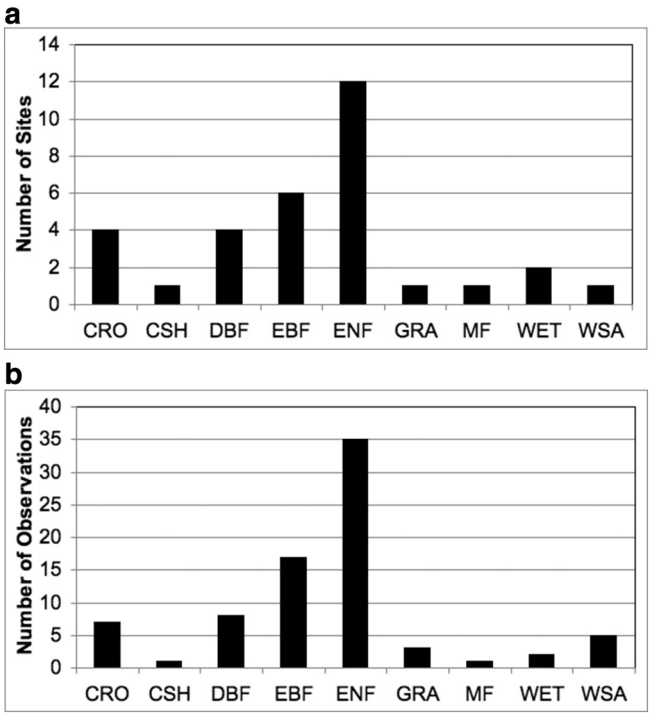

Fig. 3. a. The distribution of sites used in this study by vegetation types. Codes for vegetation types are provided in caption for Table 1. There are 32 different sites.
b. The distribution of spectral observations used in this study by vegetation types. Codes for vegetation types are provided in caption for Table 1. There are a total of 79 observations.

band with Fig. 4 showing the R^2 between each band reflectance and daily LUE for all bands. None of the individual band reflectances performed well as descriptors of daily LUE, with R^2 near zero for bands between 1185 and 1235 nm and the best performing band in the shortwave infrared (SWIR) at 2375 nm ($R^2 = 0.258$). Generally, individual SWIR bands had better performance than the visible and near infrared bands, with no band between 488 nm, the minimum usable wavelength band, and 1346 nm having a $R^2 > 0.220$, while SWIR bands from 1508 to 1558 nm and 2093 to 2375 nm all produced a $R^2 > 0.220$.

Derivatives of the spectral reflectance can be used as SVI. Derivatives are sensitive to changes in the curvature of the spectrum, changes which are mainly related to chemical and physical changes in vegetation canopies, but not sensitive to variations in brightness, so they act to dampen these potential sources of noise, such as soil background reflectance variations (Hall et al., 1990). In some spectral regions, the first derivatives of the reflectance spectrum performed far better than the corresponding individual band reflectances, as shown in Fig. 4, with a R^2 as high as 0.467 at 742 nm in the red edge region of the spectrum. This is a larger R^2 than Dmax, the maximum first derivative (Dmax $R^2 = 0.351$), which has been related to plant health, nitrogen content, and GEP (Campbell et al., 2004, 2013). Other spectral regions where the first derivative performs better than individual band reflectance (where $R^2 > 0.3$) include: 610–620 nm (edge of green peak), 732–783 nm (red edge region), both responding to vegetation chlorophyll content; and 1235 nm, 1558–1578 nm, 1750–1760 nm, and 2113–2123 nm, all spectral bands on the edge of water absorption features responding to leaf water content. A SVI made up of the ratio of the first derivatives of the reflectance spectra at 730 nm and 706 nm performed better than the derivative of any single band, achieving a R^2 of 0.516 and a SE of 0.00741 mol CO_2 mol^{-1} absorbed photons (Fig. 5) (Entcheva et al., 2004, Campbell et al., 2007).

A common form for a SVI is a two band normalized difference vegetation index which is the difference between the two bands divided by their sum. Normalized difference indices were developed to reduce effects of brightness differences among scenes, again minimizing sources of variability that are not due to the variable being measured, in this case LUE (Rouse et al., 1973; Tucker, 1979). Normalized difference vegetation indices were calculated for all two-band combinations resulting in 8778 different combinations that were tested against LUE. Fig. 6 shows patterns of R^2 for the different band combinations and Table 2 provides a list of the 20 best-performing two-band normalized difference indices. Spectral regions with higher R^2 values appear as red areas in Fig. 6; these areas cover a wide range of spectral bands with 60 different bands being used in indices with $R^2 > 0.45$. Spectral regions for indices with higher R^2 values include bands at 722 and 732 nm combined with bands at 742 through 925 nm, indices responding to spectral curvature changes near the red edge mainly determined by plant chlorophyll content; bands at 1528 through 1568 nm combined with bands 1578 through 1750 nm and the 1770 nm band combined with bands at 1730 and 1740 nm, spectral regions affected by leaf water content; the 1185 nm band combined with bands at 1286 and 1296 nm, bands 783 through 925 nm combined with bands 1255 through

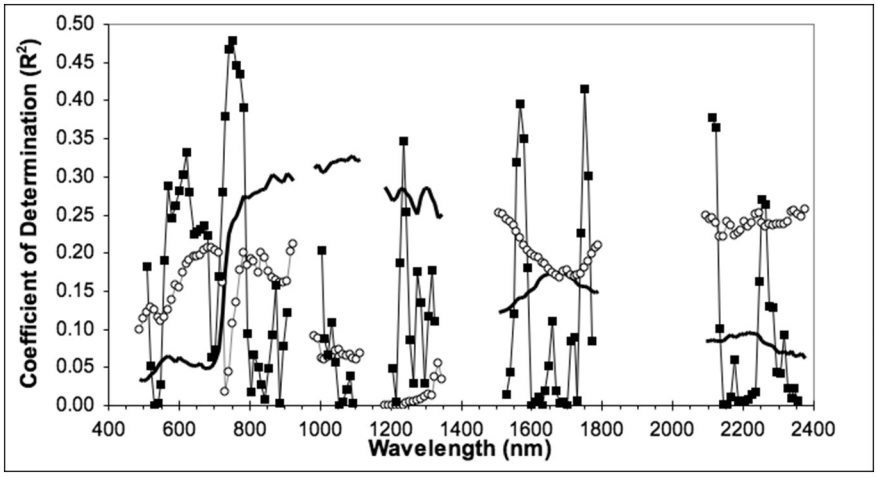

Fig. 4. For linear relationships with daily LUE the R^2 for each band reflectance (open circles) and the first derivative (solid black squares). Gray line is average spectral reflectance for reference.

1306 nm, and bands 983 and 1033 nm combined with bands 1276 through 1306 nm, spectral bands affected by leaf structure and water content. Specifically, indices using bands at 732, 1548, or 1720 nm and neighboring bands turn up multiple times in the top 20 performing indices (Table 2). Figs. 7 and 8 show the relationships of two of the best performing two band normalized difference indices, using bands at 732 and 742 nm and bands at 1548 and 1740 nm respectively, plotted with daily LUE.

Some of the two band normalized difference indices are noteworthy as they have been previously described in the literature. These include the Normalized Difference Vegetation Index (NDVI) (Tucker, 1979) using bands at 681 and 773 nm, yielding a R^2 of 0.292 and SE of 0.00897 mol CO_2 mol^{-1} absorbed photons; the Normalized Difference Infrared Index (NDII) (Jackson et al., 2004) using bands at 819 and1649 nm, producing a R^2 of 0.326 and SE of 0.00875 mol CO_2 mol^{-1} absorbed photons; and the Normalized Difference Water Index (NDWI) (Gao, 1996) using bands at 870 and 1240 nm, with a R^2 of 0.417 and SE of 0.00813 mol CO_2 mol^{-1} absorbed photons.

The PRI, the normalized difference of a band near 531 nm and a reference band usually at 570 nm, is particularly interesting as it has been shown to be related to LUE in several studies (e.g. Nichol et al., 2000, Gamon et al., 1997, Penuelas et al., 1995). The nearest Hyperion bands for PRI are centered at 529 nm and 569 nm, and this band combination performs poorly with a R^2 of 0.029 and SE of 0.01050 mol CO_2 mol^{-1} absorbed photons (Fig. 9). Low values of PRI correspond with low LUE values, however with increasing PRI the range of possible LUEs gets wider. Landscape characteristics such as varying leaf area or shadows can affect PRI (Barton and North, 2001). Other studies of PRI suggest that the relationship between PRI and LUE vary for different sites and vegetation types (Drolet et al., 2008; Middleton et al., 2016) and this effect is hinted at in Fig. 9 with crops having a steep slope between PRI and LUE, while the deciduous and evergreen broadleaf forests have smaller slopes, and evergreen needleleaf forests having middle values for slopes. These site differences lead to the poor overall performance of PRI for all sites combined.

While a band near 570 nm has usually been used as the PRI reference band, we can examine the performance of other reference bands. The best performing reference band for PRI was at 671 nm with a R^2 of 0.203. The use of this red spectral band is similar to versions of PRI using MODIS bands where the reference band is MODIS band 1, centered at 645 nm. This version of MODIS PRI is sometimes referred to as the Chlorophyll-Carotenoid Index (CCI) and has been related to the seasonally changing ratio of chlorophyll to carotenoid pigment pools and GEP in boreal conifers (Wong and Gamon, 2015; Gamon et al., 2016).

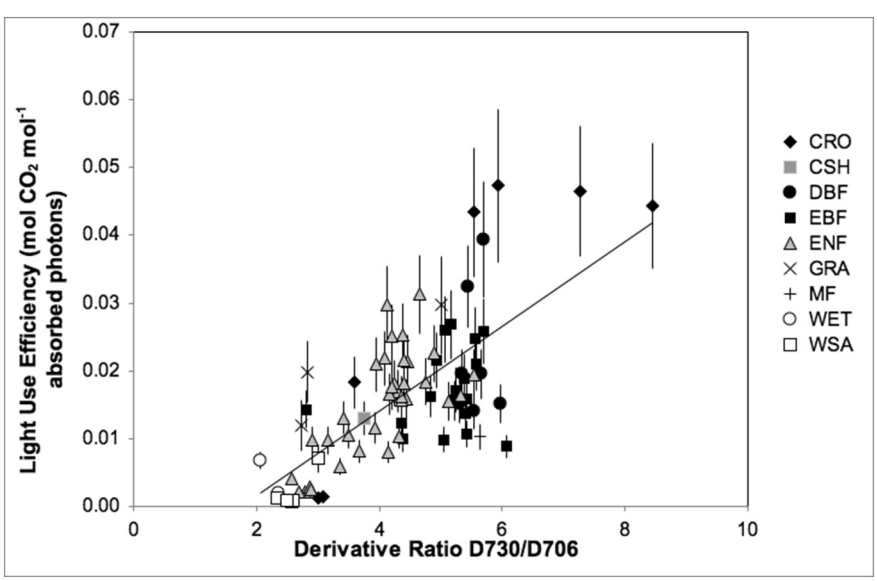

Fig. 5. The ratio of the first derivatives of the reflectance spectra at 730 nm and 706 nm versus daily LUE. This was the best performing SVI with a R^2 to LUE of 0.516 and a SE of 0.00741 mol CO_2 mol^{-1} absorbed photons for all points. The symbols indicate vegetation type reported for each site: filled black diamonds are crops, filled gray squares are closed shrubland, filled black circles are deciduous broadleaf forests, filled black squares are evergreen broadleaf forests, gray filled triangles are evergreen needleleaf forests, X are grassland, plus signs are mixed forests, open circles are wetlands, and open squares are woody savannahs.

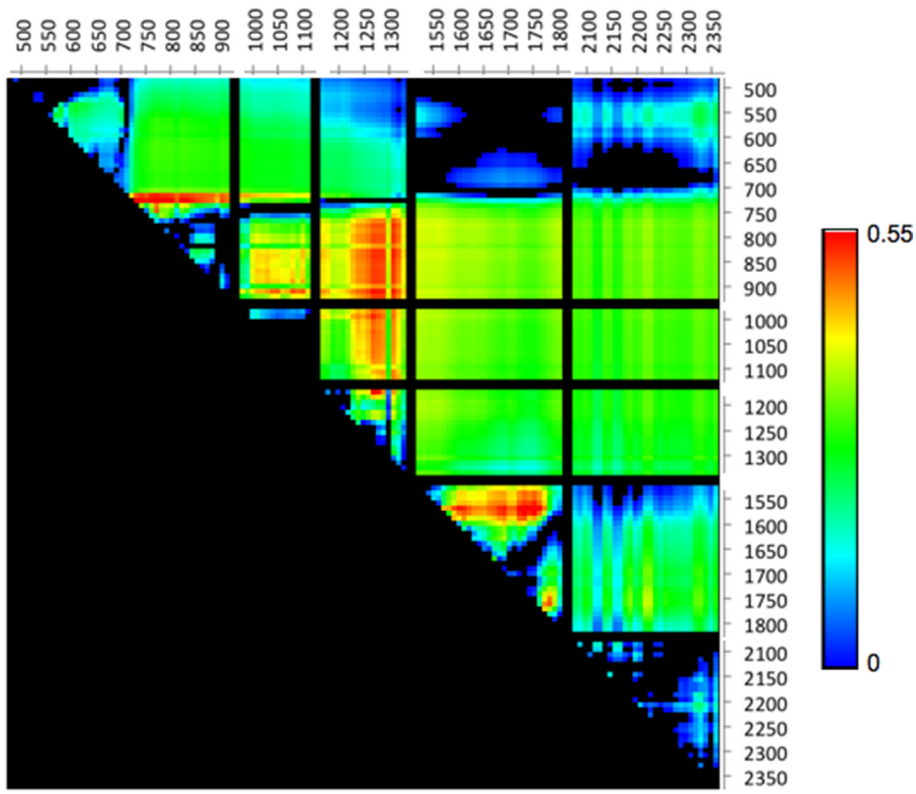

Fig. 6. Image of R^2 of two band normalized difference SVI with daily LUE. X and Y axes are wavelength bands, and the colors indicate R^2 as indicated in color bar on the right. The black bars across the image indicate where there are gaps in the Hyperion spectra due to bad detectors or atmospheric absorption.

Table 2
Best performing 2-band normalized difference indices. Columns 1 and 2 are the midpoint wavelengths for the two bands, column 3 is the coefficient of determination (R^2) with daily LUE, column 4 is the standard error of the estimate for a linear regression expressed as mol CO_2 mol^{-1} absorbed photons.

Band 1	Band 2	R^2	SE
732	742	0.548	0.00722
732	752	0.537	0.00747
732	783	0.535	0.00749
1548	1740	0.534	0.00749
732	773	0.523	0.00775
1548	1720	0.520	0.00764
1548	1730	0.514	0.00768
732	803	0.513	0.00778
732	793	0.512	0.00780
732	834	0.509	0.00770
732	813	0.505	0.00782
732	844	0.503	0.00770
1558	1720	0.501	0.00781
1548	1710	0.501	0.00774
1548	1750	0.499	0.00775
1558	1740	0.499	0.00777
1185	1286	0.499	0.00813
722	783	0.489	0.00779
1548	1588	0.489	0.00785
732	763	0.489	0.00801

3.1. PLSR results

Sixty out of the 133 spectral bands included in normalized difference indices had a $R^2 > 0.45$ (Fig. 6), indicating information related to changes in LUE are widely distributed across the spectrum. The PLSR makes use of information from all bands and produced a R^2 of 0.81 and the SE is 0.00465 mol CO_2 mol^{-1} absorbed photons for all points (Fig. 10, Table 3), far better than any of the other approaches using limited numbers of spectral bands. The weightings of the PLSR coefficients provide information on spectral regions of importance for determining LUE (Fig. 11). Generally, the wavelengths where PLSR coefficients tend to have the largest magnitudes are on the edges of spectral features. Some key wavelengths occur on the flank of the green peak at 600 nm; on the red edge at 712, 722, and 763 nm; and at the edge of water absorption bands at 1286, 1518, and 1720 nm. These same wavelength bands are also among the bands with the highest R^2 from the two band normalized difference indices, an indication of their importance in determining LUE.

The success of any statistical modeling approach depends on how well the training samples represent the entire population. The uncertainty in estimated LUE described in the random cross validation varies with sites, with most sites having a standard deviation of the cross validations of < 0.0052 mol CO_2 mol^{-1} absorbed photons. Larger uncertainties occurred in sites with vegetation types that were poorly represented in the training dataset, increasing the likelihood that they were not represented in many of the random subsets used in the cross validation. Further, the largest uncertainties occurred in cases with both the highest and lowest values of LUE. At the high end of LUE values the agricultural crop sites (US-NE2 and US-NE3) had the largest standard deviation in LUE estimations ranging between 0.0054 and 0.0137 mol CO_2 mol^{-1} absorbed photons, while low LUE cases were for sites classified as wetlands or woody savannahs (US-SRM, US-IVO, and CA-MER) with standard deviations between 0.0056 and 0.0078 mol CO_2 mol^{-1} absorbed photons.

The dataset is also weighted toward forested sites, in particular evergreen needleleaf and evergreen broadleaf forest (EBF) sites, and the significance of that bias is demonstrated in a PLSR calculation using all points except the EBF observations (Fig. 12). The RMSE for the EBF from the average of the random cross validations is 0.0043, compared to the case with no EBF in the training data with a RMSE of 0.0117 mol CO_2 mol^{-1} absorbed photons. It is clear that a reliable extension of the results of this study should expand the training dataset to include more samples from a variety of vegetation types.

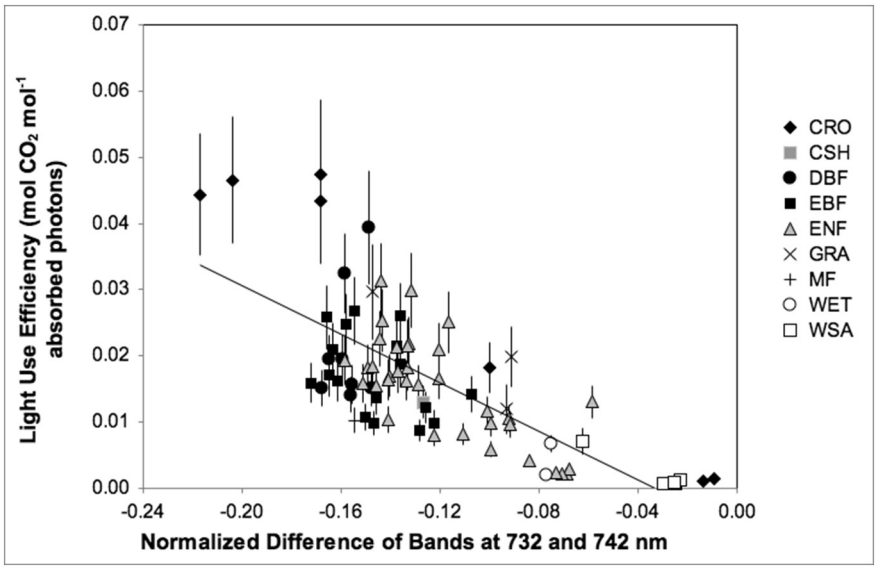

Fig. 7. The normalized difference of the 732 nm and 742 nm band reflectances versus daily LUE. This was the best performing normalized difference index (see Table 2) with a R^2 to LUE of 0.548 and a SE of 0.00722 mol CO_2 mol^{-1} absorbed photons for all points. The symbols indicate vegetation type as described in the Fig. 2 caption.

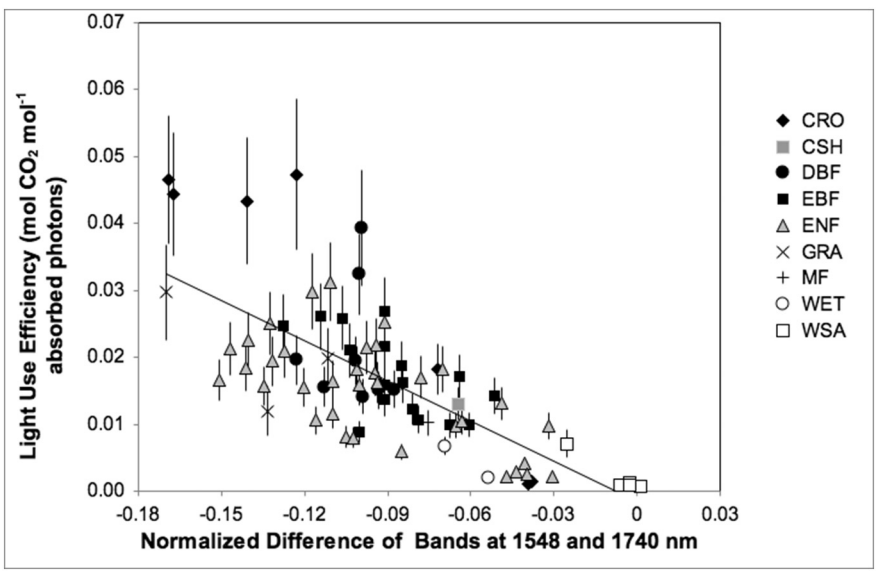

Fig. 8. The normalized difference of the 1548 nm and 1740 nm band reflectances versus daily LUE. This was the one of the best performing normalized difference indices (see Table 2) with a R^2 to LUE of 0.534 and a SE of 0.00749 mol CO_2 mol^{-1} absorbed photons for all points. The symbols indicate vegetation type as described in the Fig. 2 caption.

4. Discussion

The results of the PLSR analysis demonstrate the existence of an algorithm capable of meeting the three criteria for a successful metric across a variety of sites with multiple different vegetation types. Increasing the utilization of spectral information from two bands in the spectral derivative and SVI approaches to the entire spectra in the PLSR approach appears to decrease noise caused by site differences and provides an improved estimate of LUE. However, while widely dispersed, the available data are overrepresented in some vegetation types while missing other types because this type of data collection was not the primary mission for Hyperion. Future missions such as SBG will be able to have far more extensive coverage and thus the ability to create more comprehensive datasets for algorithm training and testing.

The potential usefulness of these retrievals can be shown through the application of the PLSR coefficients (shown in Fig. 10) to Hyperion image data to extend the results from the areas around flux towers to describe the spatial variability of LUE over a landscape. An example of an apparent LUE map derived from a Hyperion image is shown in Fig. 13 for an area near the scrub pine flux tower site in Florida, USA (US-SP3). Within that image there is wide variability in apparent LUE at the 30 m spatial resolution of Hyperion, with a nearly normal distribution of apparent LUE values, having a mean of 0.017 and a standard deviation of 0.0041 mol CO_2 mol^{-1} absorbed photons (Fig. 13). The apparent LUE varies even within an area of a square km centered on the flux tower, where the distribution ranges between 0.0099 and 0.0287, with a mean of 0.020 and standard deviation of 0.0034 mol CO_2 mol^{-1} absorbed photons (Fig. 13). This spatial variability in LUE is often not captured in light use efficiency models where spatial variability in LUE is described using weather data and land cover type, neither of which are as fine-grained as the Hyperion 30 m spectral reflectance data, so are unable to capture the spatial variability shown in Fig. 13. The improvement in the spatial mapping of LUE variations by spectral imaging provides important information for describing ecophysiological patterns and their relationship to landscape and biodiversity.

A physical reason for the success in using spectral reflectance to derive LUE is hinted at in the similarity between the spectral pattern of PLSR coefficients derived for LUE (shown in Fig. 11) and the spectral pattern of PLSR coefficients derived by Asner et al. (2015) for foliar nitrogen in tropical forest plots using imagery from aircraft. Foliar N is strongly involved in plant photochemical processes and is a key

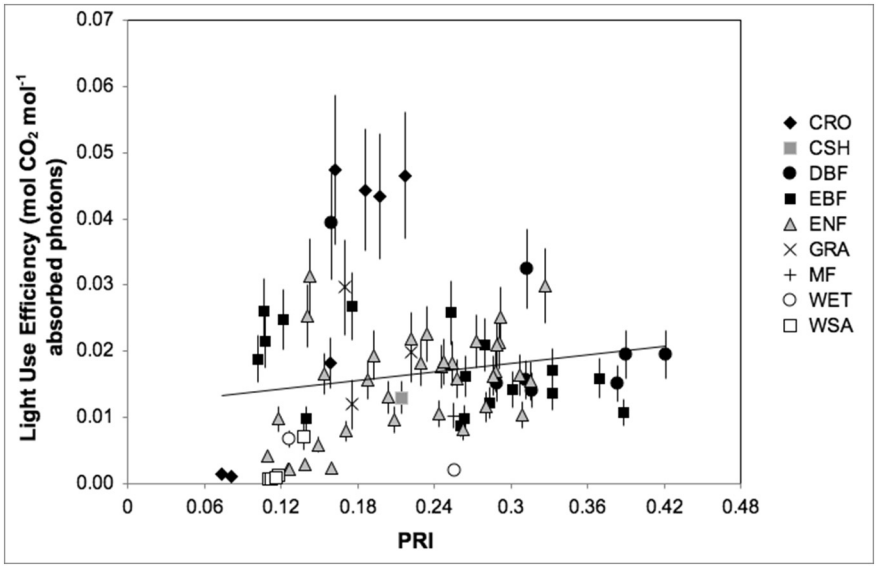

Fig. 9. The Photochemical Reflectance Index (PRI), the normalized difference of the 531 nm and 570 nm band reflectances versus daily LUE. The symbols indicate vegetation type as described in the Fig. 2 caption.

constituent of photosynthetic pigments and enzymes as well as being a component of compounds used in electron-transport (Reich, 2012; Aber et al., 1996). Most terrestrial ecosystems have evolved in N-limited environments so that increases in available N generally results in improved photosynthetic efficiency and productivity (Aber et al., 1998; Kergoat et al., 2008; Green et al., 2003). It is therefore reasonable to assume it is the ability to describe foliar N levels from spectral reflectance that underlies this study's PLSR results. It also points to the importance of collecting measurements of foliar N and spectral reflectance in conjunction with eddy covariance fluxes in a variety of different vegetation types to clarify the connections among these variables (Ollinger, 2011; Ollinger et al., 2013).

For future work in the remote sensing of LUE the available imaging spectrometers may not collect data across the full spectral range of Hyperion. For example, the DLR Earth Sensing Imaging Spectrometer (DESIS) that is flying on the International Space Station measures between 400 and 1000 nm, and imaging spectrometers that can be carried on smaller unmanned aircraft system (UAS) may have spectral ranges limited the visible to near infrared (e.g. 400–1000 nm) or shortwave infrared (e.g. 1000–2400 nm) wavelengths. To examine the potential use of spectrometers with more limited spectral ranges, the PLSR analysis described above was repeated for some subsets of the Hyperion bands (Table 3). Interestingly, cutting off the longer wavelength bands (using bands between 488 and 1790 nm) or cutting off the shorter

Table 3
Results of PLSR of LUE using different sets of wavelength bands. Column 1 describes the range of spectral bands used in the analysis and column 2 is the number of Hyperion spectral bands, column 3 is the coefficient of determination (R^2) with daily LUE, and column 4 is the standard error of the estimate for a linear regression expressed as mol CO_2 mol^{-1} absorbed photons.

Spectral range	Number of bands	R^2	SE
488–2375 nm (all bands)	133	0.81	0.00465
488–1790 nm	104	0.81	0.00467
488–1346 nm	75	0.76	0.00532
488–993 nm	46	0.69	0.00602
488–850 nm	36	0.68	0.00610
1003–2375 nm	87	0.81	0.00473
905–1599 nm	44	0.76	0.00528

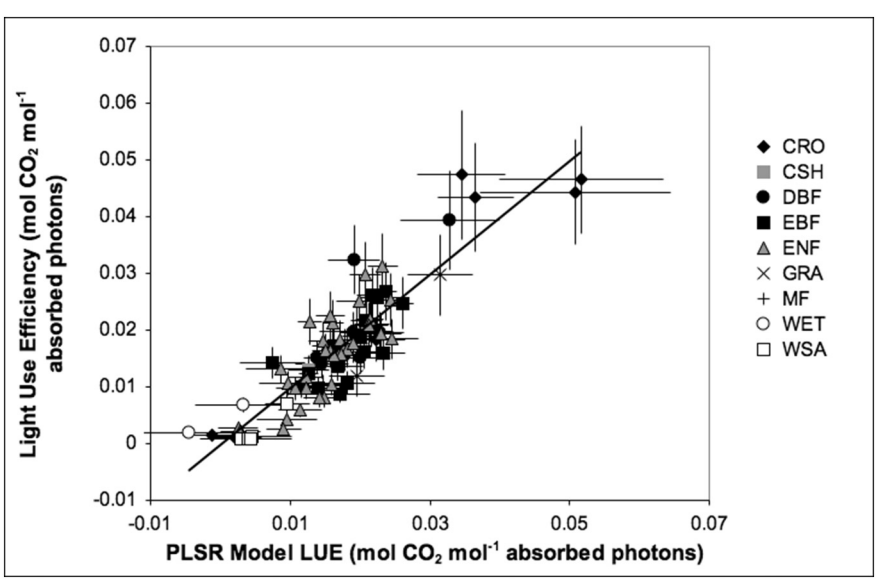

Fig. 10. LUE estimated from spectral reflectance using PLSR. Model values are the average values from all cross validation random subsets. X-axis error bars are +/− one standard deviation of values from the different subsets. The R^2 is 0.81 and the SE is 0.00465 mol CO_2 mol^{-1} absorbed photons for all points. The symbols indicate vegetation type as described in the Fig. 2 caption.

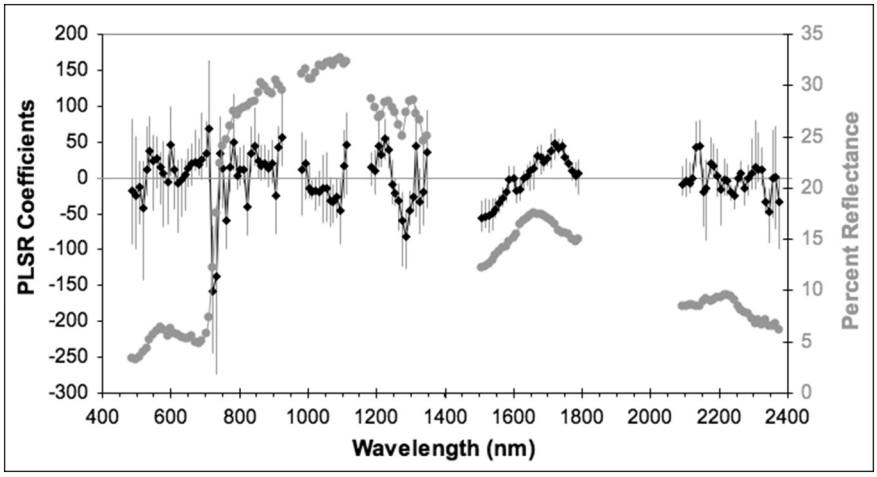

Fig. 11. Average spectral reflectance of all sites (gray points) and PLSR coefficients. The black points are the average coefficients from all the subsets, the error bars represent the maximum and minimum coefficient values from the subset regressions.

wavelength (visible to near infrared) bands (using bands between 1003 and 2375 nm) produces results as good as using all the spectral bands while eliminating significant spectral regions and using fewer bands. However, using only the visible to near infrared spectral bands significantly degrades the performance of the retrievals, dropping the R^2 to 0.68–0.69 when only using bands between 488 and 993 nm or using bands between 488 and 844 nm, in spite of the largest coefficients from the full spectra analysis occurring within these wavelength ranges. Including some of the longer wavelength bands along with the visible-near infrared bands significantly improves the R^2, increasing it to 0.76 when extending the wavelength range to 488 through 1346 nm. That same performance can be achieved without the visible-near infrared bands when using near infrared bands between 905 and 1599 nm. These results point to the importance of the middle wavelength spectral bands for determining LUE.

5. Conclusions

This examination of a variety of study sites suggests that a common global spectral approach for deriving LUE is feasible. Many two band indices based on a variety of different spectral bands showed similar performances, suggesting information related to LUE is distributed over several spectral regions. However, no two-band index had performance better than a R^2 of 0.55 with a SE > 0.0072 mol CO_2 mol^{-1} absorbed photons. By making use of information available over a range of spectral bands through PLSR, LUE retrieval performance improved to a R^2 of 0.81 with a SE of 0.0046 mol CO_2 mol^{-1} absorbed photons.

This study was made possible through the use of the Hyperion image archive, containing over 90,000 images collected over the 16-year life of its mission. The rich information content of reflectance spectra can be particularly valuable for knowledge discovery through data mining and machine learning approaches. This demonstrates how the Hyperion global dataset can be an asset for advancing remote sensing algorithm development and testing, both for upcoming missions that will be flying imaging spectrometers, such as NASA's Plankton, Aerosol, Cloud, ocean Ecosystem (PACE) and Surface Biology and Geology (SBG) missions, the German Environmental Mapping and Analysis Program (EnMAP) mission, or the Japanese Hyperspectral Imager Suite (HISUI). Further, this archive can support development of future multispectral missions, where broad spectral bands are simulated by convolving narrow hyperspectral bands, testing the use of different or additional spectral bands for possible additions to future Landsat or Sentinel missions.

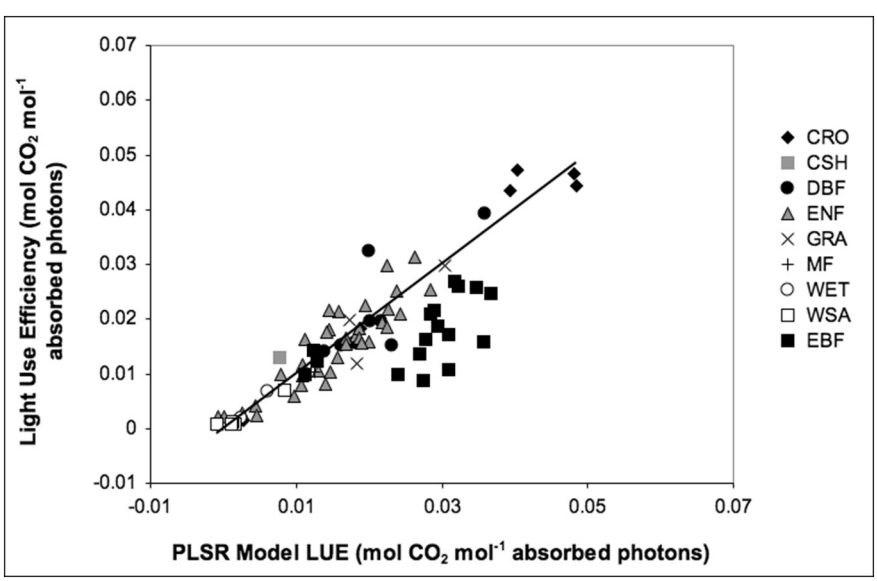

Fig. 12. LUE estimated from spectral reflectance using PLSR where the model was trained using all values but the evergreen broadleaf forest observations.

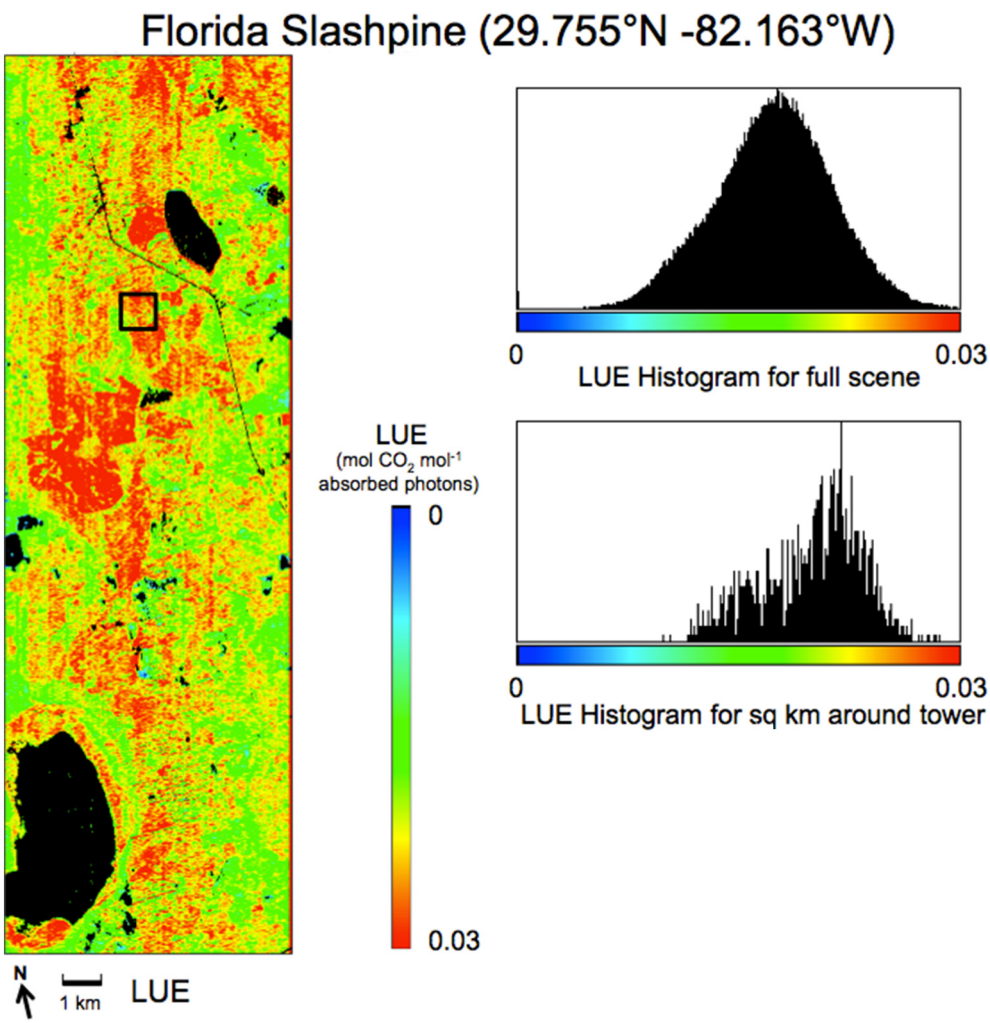

Fig. 13. Apparent LUE for the area around the Florida Slashpine flux tower site (US-SP3) mapped using the PLSR coefficients (Fig. 11) applied to a segment of a Hyperion image for October 22, 2002 (day 295). Hyperion spatial resolution is 30 m. Upper histogram shows distribution of apparent LUE values over the entire scene, the lower histogram shows distribution of apparent LUE within a 1 km^2 area around the flux tower shown as the black square on the image. LUE expressed in mol CO_2 mol^{-1} absorbed photons.

Acknowledgements

This work was supported by the NASA HyspIRI Mission Concept Preparatory Activities program.

The authors thank the FLUXNET community as this type of analysis would not be possible without their support of a global network of eddy covariance flux towers and their efforts to process and make these data available, in particular by the following networks: AmeriFlux (U.S. Department of Energy, Biological and Environmental Research, Terrestrial Carbon Program (DE-FG02-04ER63917 and DE-FG02-04ER63911)), AfriFlux, AsiaFlux, CarboAfrica, CarboEuropeIP, CarboItaly, CarboMont, ChinaFlux, Fluxnet-Canada (supported by CFCAS, NSERC, BIOCAP, Environment Canada, and NRCan), GreenGrass, KoFlux, LBA, NECC, OzFlux, TCOS-Siberia, USCCC. We acknowledge the financial support to the eddy covariance data harmonization provided by CarboEuropeIP, FAO-GTOS-TCO, iLEAPS, Max Planck Institute for Biogeochemistry, National Science Foundation, University of Tuscia, Université Laval, Environment Canada and US Department of Energy and the database development and technical support from Berkeley Water Center, Lawrence Berkeley National Laboratory, Microsoft Research eScience, Oak Ridge National Laboratory, University of California-Berkeley and the University of Virginia.

The authors wish to specifically thank the providers of the flux data: Akira Miyata, Alan Barr, Alessandro Araujo, Andrew Richardson, Bert Drake, Bill Munger, David Hollinger, Eva van Gorsel, Harry McCaughey, Julian Hadley, Laonardo Sa, Mike Goulden, Mike Jones, Peter Lafleur, Russ Scott, Scott Saleska, Serge Rambal, Richard Joffre, Shashi Verma, T. Andrew Black, Tilden Meyers, Tim Martin, Rosvel Bracho, Walt Oechel, Donatella Zona, and Xudong Zhang.

References

Aber, J.D., Reich, P.B., Goulden, M.L., 1996. Extrapolating leaf CO_2 exchange to the canopy: a generalized model of forest photosynthesis compared with measurements by eddy correlation. Oecologia 106 (2), 257–265. https://doi.org/10.1007/BF00328606.

Aber, J., McDowell, W., Nadelhoffer, K., Magill, A., Berntson, G., Kamakea, M., McNulty, S., Currie, W., Rustad, L., Fernandez, I., 1998. Nitrogen saturation in temperate forest ecosystems. BioScience 48 (11), 921–934. https://doi.org/10.2307/1313296.

Agarwal, D.A., Humphrey, M., Beekwilder, N.F., Jackson, K.R., Goode, M.M., van Ingen, C., 2010. A data-centered collaboration portal to support global carbon-flux analysis. Concurrency and Computation: Practice and Experience 22 (17), 2323–2334. https://doi.org/10.1002/cpe.1600.

Araújo, A.C., Nobre, A.D., Kruijt, B., Elbers, J.A., Dallarosa, R., Stefani, P., Von Randow, C., Manzi, A.O., Culf, A.D., Gash, J.H.C., Valentini, R., 2002. Comparative measurements of carbon dioxide fluxes from two nearby towers in a central Amazonian rainforest: the Manaus LBA site. Journal of Geophysical Research: Atmospheres 107 (D20), 72–88. https://doi.org/10.1029/2001JD000676.

Asner, G.P., Martin, R.E., Anderson, C.B., Knapp, D.E., 2015. Quantifying forest canopy traits: imaging spectroscopy versus field survey. Remote Sens. Environ. 158, 15–27. https://doi.org/10.1016/j.rse.2014.11.011.

Baker, T.R., Phillips, O.L., Malhi, Y., Almeida, S., Arroyo, L., Di Fiore, A., Erwin, T., Killeen, T.J., Laurance, S.G., Laurance, W.F., Lewis, S.L., 2004. Variation in wood density determines spatial patterns in Amazonian forest biomass. Glob. Chang. Biol. 10 (5), 545–562. https://doi.org/10.1111/j.1365-2486.2004.00751.x.

Baldocchi, D., 2008. 'Breathing' of the terrestrial biosphere: lessons learned from a global network of carbon dioxide flux measurement systems. Aust. J. Bot. 56 (1), 1–26. https://doi.org/10.1071/BT07151.

Baldocchi, D.D., Vogel, C.A., Hall, B., 1997. Seasonal variation of energy and water vapor exchange rates above and below a boreal jack pine forest canopy. Journal of Geophysical Research: Atmospheres 102 (D24), 28939–28951. https://doi.org/10.1029/96JD03325.

Barton, C.V.M., North, P.R.J., 2001. Remote sensing of canopy light use efficiency using the photochemical reflectance index: model and sensitivity analysis. Remote Sens. Environ. 78 (3), 264–273. https://doi.org/10.1016/S0034-4257(01)00224-3.

Bond-Lamberty, B., Wang, C., Gower, S.T., 2004. Net primary production and net ecosystem production of a boreal black spruce wildfire chronosequence. Glob. Chang. Biol. 10 (4), 473–487. https://doi.org/10.1111/j.1529-8817.2003.0742.x.

Boulesteix, A.L., Strimmer, K., 2006. Partial least squares: a versatile tool for the analysis of high-dimensional genomic data. Brief. Bioinform. 8 (1), 32–44. https://doi.org/10.1093/bib/bbl016.

Bracho, R., Powell, T.L., Dore, S., Li, J., Hinkle, C.R., Drake, B.G., 2008. Environmental and biological controls on water and energy exchange in Florida scrub oak and pine flatwoods ecosystems. Journal of Geophysical Research: Biogeosciences 113 (G2). https://doi.org/10.1029/2007JG000469.

Campbell, P.E., Rock, B.N., Martin, M.E., Neefus, C.D., Irons, J.R., Middleton, E.M., Albrechtova, J., 2004. Detection of initial damage in Norway spruce canopies using hyperspectral airborne data. Int. J. Remote Sens. 25 (24), 5557–5584. https://doi.org/10.1080/01431160410001726058.

Campbell, P.K.E., Middleton, E.M., McMurtrey, J.E., Chappelle, E.W., 2007. Assessment of vegetation stress using reflectance or fluorescence measurements. J. Environ. Qual. 36 (3), 832–845. https://doi.org/10.2134/jeq2005.0396.

Campbell, P.K.E., Middleton, E.M., Thome, K.J., Kokaly, R.F., Huemmrich, K.F., Lagomasino, D., Novick, K.A., Brunsell, N.A., 2013. EO-1 Hyperion reflectance time series at calibration and validation sites: stability and sensitivity to seasonal dynamics. IEEE Journal of Selected Topics in Applied Earth Observations and Remote Sensing 6 (2), 276–290. https://doi.org/10.1109/JSTARS.2013.2246139.

Carswell, F.E., Costa, A.L., Palheta, M., Malhi, Y., Meir, P., Costa, J.D.P.R., Ruivo, M.D.L., Leal, L.D.S.M., Costa, J.M.N., Clement, R.J., Grace, J., 2002. Seasonality in CO2 and H2O flux at an eastern Amazonian rain forest. Journal of Geophysical Research: Atmospheres 107 (D20), 8076. https://doi.org/10.1029/2000JD000284.

Ciais, P., Dolman, A.J., Bombelli, A., Duren, R., Peregon, A., Rayner, P.J., Miller, C., Gobron, N., Kinderman, G., Marland, G., Gruber, N., 2014. Current systematic carbon-cycle observations and the need for implementing a policy-relevant carbon observing system. Biogeosciences 11, 3547–3602. https://doi.org/10.5194/bg-11-3547-2014.

Clark, K.L., Gholz, H.L., Moncrieff, J.B., Cropley, F., Loescher, H.W., 1999. Environmental controls over net exchanges of carbon dioxide from contrasting Florida ecosystems. Ecol. Appl. 9 (3), 936–948. https://doi.org/10.1890/1051-0761(1999)009[0936:ECONEO]2.0.CO;2.

Clark, K.L., Gholz, H.L., Castro, M.S., 2004. Carbon dynamics along a chronosequence of slash pine plantations in north Florida. Ecol. Appl. 14 (4), 1154–1171. https://doi.org/10.1890/02-5391.

Coops, N.C., Hilker, T., Hall, F.G., Nichol, C.J., Drolet, G.G., 2010. Estimation of light-use efficiency of terrestrial ecosystems from space: a status report. BioScience 60 (10), 788–797. https://doi.org/10.1525/bio.2010.60.10.5.

Coursolle, C., Margolis, H.A., Barr, A.G., Black, T.A., Amiro, B.D., McCaughey, J.H., Flanagan, L.B., Lafleur, P.M., Roulet, N.T., Bourque, C.P.A., Arain, M.A., 2006. Late-summer carbon fluxes from Canadian forests and peatlands along an east west continental transect. Can. J. For. Res. 36 (3), 783–800. https://doi.org/10.1139/x05-270.

Da Rocha, H.R., Goulden, M.L., Miller, S.D., Menton, M.C., Pinto, L.D., de Freitas, H.C., 2004. Seasonality of water and heat fluxes over a tropical forest in eastern Amazonia. Ecol. Appl. 14 (sp4), 22–32. https://doi.org/10.1890/02-6001.

Davidson, E.A., Richardson, A.D., Savage, K.E., Hollinger, D.Y., 2006. A distinct seasonal pattern of the ratio of soil respiration to total ecosystem respiration in a spruce-dominated forest. Glob. Chang. Biol. 12 (2), 230–239. https://doi.org/10.1111/j.1365-2486.2005.01062.x.

Dawson, T.P., North, P.R.J., Plummer, S.E., Curran, P.J., 2003. Forest ecosystem chlorophyll content: implications for remotely sensed estimates of net primary productivity. Int. J. Remote Sens. 24 (3), 611–617. https://doi.org/10.1080/01431160304984.

Drolet, G.G., Middleton, E.M., Huemmrich, K.F., Hall, F.G., Amiro, B.D., Barr, A.G., Black, T.A., McCaughey, J.H., Margolis, H.A., 2008. Regional mapping of gross light-use efficiency using MODIS spectral indices. Remote Sens. Environ. 112 (6), 3064–3078. https://doi.org/10.1016/j.rse.2008.03.002.

Fang, H., Li, W., Myneni, R.B., 2013. The impact of potential land cover misclassification on MODIS leaf area index (LAI) estimation: a statistical perspective. Remote Sens. 5 (2), 830–844. https://doi.org/10.3390/rs5020830.

Friedl, M.A., Sulla-Menashe, D., Tan, B., Schneider, A., Ramankutty, N., Sibley, A., Huang, X., 2010. MODIS Collection 5 global land cover: algorithm refinements and characterization of new datasets. Remote Sens. Environ. 114 (1), 168–182. https://doi.org/10.1016/j.rse.2009.08.016.

Friend, A.D., Lucht, W., Rademacher, T.T., Keribin, R., Betts, R., Cadule, P., Ciais, P., Clark, D.B., Dankers, R., Falloon, P.D., Ito, A., 2014. Carbon residence time dominates uncertainty in terrestrial vegetation responses to future climate and atmospheric CO_2. Proc. Natl. Acad. Sci. 111 (9), 3280–3285. https://doi.org/10.1073/pnas.1222477110.

Gamon, J.A., 2015. Reviews and syntheses: optical sampling of the flux tower footprint. Biogeosciences 12 (14), 4509–4523. https://doi.org/10.5194/bg-12-4509-2015.

Gamon, J., Serrano, L., Surfus, J.S., 1997. The photochemical reflectance index: an optical indicator of photosynthetic radiation use efficiency across species, functional types, and nutrient levels. Oecologia 112 (4), 492–501. https://doi.org/10.1007/s004420050337.

Gamon, J.A., Huemmrich, K.F., Wong, C.Y., Ensminger, I., Garrity, S., Hollinger, D.Y., Noormets, A., Peñuelas, J., 2016. A remotely sensed pigment index reveals photosynthetic phenology in evergreen conifers. Proc. Natl. Acad. Sci. 113 (46), 13087–13092. https://doi.org/10.1073/pnas.1606162113.

Gao, B.C., 1996. NDWI—A normalized difference water index for remote sensing of vegetation liquid water from space. Remote Sens. Environ. 58 (3), 257–266. https://doi.org/10.1016/S0034-4257(96)00067-3.

Gao, B.C., Davis, C.O., 1997. Development of a line-by-line-based atmosphere removal algorithm for airborne and spaceborne imaging spectrometers. In: Imaging Spectrometry III. Vol. 3118. International Society for Optics and Photonics, pp. 132–142. https://doi.org/10.1117/12.283822. October.

Gao, B.C., Montes, M.J., Davis, C.O., Goetz, A.F., 2009. Atmospheric correction algorithms for hyperspectral remote sensing data of land and ocean. Remote Sens. Environ. 113, S17–S24. https://doi.org/10.1016/j.rse.2007.12.015.

Garbulsky, M.F., Peñuelas, J., Gamon, J., Inoue, Y., Filella, I., 2011. The photochemical reflectance index (PRI) and the remote sensing of leaf, canopy and ecosystem radiation use efficiencies: a review and meta-analysis. Remote Sens. Environ. 115 (2), 281–297. https://doi.org/10.1016/j.rse.2010.08.023.

Gilmanov, T.G., Tieszen, L.L., Wylie, B.K., Flanagan, L.B., Frank, A.B., Haferkamp, M.R., Meyers, T.P., Morgan, J.A., 2005. Integration of CO2 flux and remotely-sensed data for primary production and ecosystem respiration analyses in the Northern Great Plains: potential for quantitative spatial extrapolation. Glob. Ecol. Biogeogr. 14 (3), 271–292. https://doi.org/10.1111/j.1466-822X.2005.00151.x.

Gilmanov, T.G., Soussana, J.F., Aires, L., Allard, V., Ammann, C., Balzarolo, M., Barcza, Z., Bernhofer, C., Campbell, C.L., Cernusca, A., Cescatti, A., 2007. Partitioning European grassland net ecosystem CO2 exchange into gross primary productivity and ecosystem respiration using light response function analysis. Agric. Ecosyst. Environ. 121 (1–2), 93–120. https://doi.org/10.1016/j.agee.2006.12.008.

Goulden, M.L., Winston, G.C., McMillan, A., Litvak, M.E., Read, E.L., Rocha, A.V., Rob Elliot, J., 2006. An eddy covariance mesonet to measure the effect of forest age on land–atmosphere exchange. Glob. Chang. Biol. 12 (11), 2146–2162. https://doi.org/10.1111/j.1365-2486.2006.01251.x.

Goward, S.N., Huemmrich, K.F., 1992. Vegetation canopy PAR absorptance and the normalized difference vegetation index: an assessment using the SAIL model. Remote Sens. Environ. 39 (2), 119–140. https://doi.org/10.1016/0034-4257(92)90131-3.

Grace, J., Nichol, C., Disney, M., Lewis, P., Quaife, T., Bowyer, P., 2007. Can we measure terrestrial photosynthesis from space directly, using spectral reflectance and fluorescence? Glob. Chang. Biol. 13 (7), 1484–1497. https://doi.org/10.1111/j.1365-2486.2007.01352.x.

Green, D.S., Erickson, J.E., Kruger, E.L., 2003. Foliar morphology and canopy nitrogen as predictors of light-use efficiency in terrestrial vegetation. Agric. For. Meteorol. 115 (3–4), 163–171. https://doi.org/10.1016/S0168-1923(02)00210-1.

Hall, F.G., Huemmrich, K.F., Goward, S.N., 1990. Use of narrow-band spectra to estimate the fraction of absorbed photosynthetically active radiation. Remote Sens. Environ. 32 (1), 47–54. https://doi.org/10.1016/0034-4257(90)90097-6.

Herold, M., Mayaux, P., Woodcock, C.E., Baccini, A., Schmullius, C., 2008. Some challenges in global land cover mapping: an assessment of agreement and accuracy in existing 1 km datasets. Remote Sens. Environ. 112 (5), 2538–2556. https://doi.org/10.1016/j.rse.2007.11.013.

Hilker, T., Coops, N.C., Wulder, M.A., Black, T.A., Guy, R.D., 2008. The use of remote sensing in light use efficiency based models of gross primary production: a review of current status and future requirements. Sci. Total Environ. 404 (2–3), 411–423. https://doi.org/10.1016/j.scitotenv.2007.11.007.

Hoffman, F.M., Randerson, J.T., Arora, V.K., Bao, Q., Cadule, P., Ji, D., Jones, C.D., Kawamiya, M., Khatiwala, S., Lindsay, K., Obata, A., 2014. Causes and implications of persistent atmospheric carbon dioxide biases in Earth System Models. Journal of Geophysical Research: Biogeosciences 119 (2), 141–162. https://doi.org/10.1002/2013JG002381.

Hollinger, D.Y., Goltz, S.M., Davidson, E.A., Lee, J.T., Tu, K., Valentine, H.T., 1999. Seasonal patterns and environmental control of carbon dioxide and water vapour exchange in an ecotonal boreal forest. Glob. Chang. Biol. 5 (8), 891–902. https://doi.org/10.1046/j.1365-2486.1999.00281.x.

Houborg, R., Anderson, M.C., Daughtry, C.S.T., Kustas, W.P., Rodell, M., 2011. Using leaf chlorophyll to parameterize light-use-efficiency within a thermal-based carbon, water and energy exchange model. Remote Sens. Environ. 115 (7), 1694–1705. https://doi.org/10.1016/j.rse.2011.02.027.

Huemmrich, K.F., Goward, S.N., 1997. Vegetation canopy PAR absorptance and NDVI: an assessment for ten tree species with the SAIL model. Remote Sens. Environ. 61 (2), 254–269. https://doi.org/10.1016/S0034-4257(97)00042-4.

Huemmrich, K.F., Gamon, J.A., Tweedie, C.E., Campbell, P.K.E., Landis, D.R., Middleton, E.M., 2013. Arctic tundra vegetation functional types based on photosynthetic physiology and optical properties. IEEE Journal of Selected Topics in Applied Earth Observations and Remote Sensing 6 (2), 265–275. https://doi.org/10.1109/JSTARS.2013.2253446.

Huemmrich, K.F., Campbell, P.K.E., Gao, B.C., Flanagan, L.B., Goulden, M., 2017. ISS as a platform for optical remote sensing of ecosystem carbon fluxes: a case study using HICO. IEEE Journal of Selected Topics in Applied Earth Observations and Remote Sensing 10 (10), 4360–4375. https://doi.org/10.1109/JSTARS.2017.2725825.

Humphreys, E.R., Black, T.A., Ethier, G.J., Drewitt, G.B., Spittlehouse, D.L., Jork, E.M.,

Nesic, Z., Livingston, N.J., 2003. Annual and seasonal variability of sensible and latent heat fluxes above a coastal Douglas-fir forest, British Columbia, Canada. Agric. For. Meteorol. 115 (1–2), 109–125. https://doi.org/10.1016/S0168-1923(02)00171-5.

Humphreys, E.R., Black, T.A., Morgenstern, K., Cai, T., Drewitt, G.B., Nesic, Z., Trofymow, J.A., 2006. Carbon dioxide fluxes in coastal Douglas-fir stands at different stages of development after clearcut harvesting. Agric. For. Meteorol. 140 (1–4), 6–22. https://doi.org/10.1016/j.agrformet.2006.03.018.

Jackson, T.J., Chen, D., Cosh, M., Li, F., Anderson, M., Walthall, C., Doriaswamy, P., Hunt, E.R., 2004. Vegetation water content mapping using Landsat data derived normalized difference water index for corn and soybeans. Remote Sens. Environ. 92 (4), 475–482. https://doi.org/10.1016/j.rse.2003.10.021.

Jung, M., Vetter, M., Herold, M., Churkina, G., Reichstein, M., Zaehle, S., Ciais, P., Viovy, N., Bondeau, A., Chen, Y., Trusilova, K., 2007. Uncertainties of modeling gross primary productivity over Europe: a systematic study on the effects of using different drivers and terrestrial biosphere models. Glob. Biogeochem. Cycles 21 (4). https://doi.org/10.1029/2006GB002915.

Kergoat, L., Lafont, S., Arneth, A., Le Dantec, V., Saugier, B., 2008. Nitrogen controls plant canopy light-use efficiency in temperate and boreal ecosystems. Journal of Geophysical Research: Biogeosciences 113 (G4). https://doi.org/10.1029/2007JG000676.

Kotchenova, S.Y., Vermote, E.F., Matarrese, R., Klemm Jr., F.J., 2006. Validation of a vector version of the 6S radiative transfer code for atmospheric correction of satellite data. Part I: path radiance. Appl. Opt. 45 (26), 6762–6774. https://doi.org/10.1364/AO.45.006762.

Lafleur, P.M., Roulet, N.T., Bubier, J.L., Frolking, S., Moore, T.R., 2003. Interannual variability in the peatland-atmosphere carbon dioxide exchange at an ombrotrophic bog. Glob. Biogeochem. Cycles 17 (2). https://doi.org/10.1029/2002GB001983.

Leuning, R., Cleugh, H.A., Zegelin, S.J., Hughes, D., 2005. Carbon and water fluxes over a temperate Eucalyptus forest and a tropical wet/dry savanna in Australia: measurements and comparison with MODIS remote sensing estimates. Agric. For. Meteorol. 129 (3–4), 151–173. https://doi.org/10.1016/j.agrformet.2004.12.004.

Lin, J.C., Pejam, M.R., Chan, E., Wofsy, S.C., Gottlieb, E.W., Margolis, H.A., McCaughey, J.H., 2011. Attributing uncertainties in simulated biospheric carbon fluxes to different error sources. Glob. Biogeochem. Cycles 25 (2). https://doi.org/10.1029/2010GB003884.

Lotsch, A., Tian, Y., Friedl, M.A., Myneni, R.B., 2003. Land cover mapping in support of LAI and FPAR retrievals from EOS-MODIS and MISR: classification methods and sensitivities to errors. Int. J. Remote Sens. 24 (10), 1997–2016. https://doi.org/10.1080/01431160210154858.

Magill, A.H., Aber, J.D., Currie, W.S., Nadelhoffer, K.J., Martin, M.E., McDowell, W.H., Melillo, J.M., Steudler, P., 2004. Ecosystem response to 15 years of chronic nitrogen additions at the Harvard Forest LTER, Massachusetts, USA. For. Ecol. Manag. 196 (1), 7–28. https://doi.org/10.1016/j.foreco.2004.03.033.

Martel, M.C., Margolis, H.A., Coursolle, C., Bigras, F.J., Heinsch, F.A., Running, S.W., 2005. Decreasing photosynthesis at different spatial scales during the late growing season on a boreal cutover. Tree Physiol. 25 (6), 689–699. https://doi.org/10.1093/treephys/25.6.689.

Martin, M.E., Plourde, L.C., Ollinger, S.V., Smith, M.L., McNeil, B.E., 2008. A generalizable method for remote sensing of canopy nitrogen across a wide range of forest ecosystems. Remote Sens. Environ. 112 (9), 3511–3519. https://doi.org/10.1016/j.rse.2008.04.008.

McCaughey, J.H., Pejam, M.R., Arain, M.A., Cameron, D.A., 2006. Carbon dioxide and energy fluxes from a boreal mixedwood forest ecosystem in Ontario, Canada. Agric. For. Meteorol. 140 (1–4), 79–96. https://doi.org/10.1016/j.agrformet.2006.08.010.

McEwing, K.R., Fisher, J.P., Zona, D., 2015. Environmental and vegetation controls on the spatial variability of CH 4 emission from wet-sedge and tussock tundra ecosystems in the Arctic. Plant Soil 388 (1–2), 37–52. https://doi.org/10.1007/s11104-014-2377-1.

Mevik, B.-H., Wehren, R., 2007. The pls package: principal component and partial least squares regression in R. J. Stat. Softw. 18 (2), 1–23. https://doi.org/10.18637/jss.v018.i02.

Michalak, A.M., Jackson, R.B., Marland, G., Sabine, C., 2011. A US Carbon Cycle Science Plan. https://www.carboncyclescience.us/USCarbonCycleSciencePlan-August2011.

Middleton, E.M., Huemmrich, K.F., Cheng, Y.-B., Margolis, H.A., 2011. Spectral bio-indicators of photosynthetic efficiency and vegetation stress. In: Thenkabail, P.S., Lyon, J.G., Huete, A. (Eds.), Hyperspectral Remote Sensing of Vegetation. CRC Press (ISBN-10: 1439845379).

Middleton, E.M., Ungar, S.G., Mandl, D.J., Ong, L., Frye, S.W., Campbell, P.E., Landis, D.R., Young, J.P., Pollack, N.H., 2013. The earth observing one (EO-1) satellite mission: over a decade in space. IEEE Journal of Selected Topics in Applied Earth Observations and Remote Sensing 6 (2), 243–256. https://doi.org/10.1109/JSTARS.2013.2249496.

Middleton, E.M., Huemmrich, K.F., Landis, D.R., Black, T.A., Barr, A.G., McCaughey, J.H., 2016. Photosynthetic efficiency of northern forest ecosystems using a MODIS-derived photochemical reflectance index (PRI). Remote Sens. Environ. 187, 345–366. https://doi.org/10.1016/j.rse.2016.10.021.

Moffat, A.M., Papale, D., Reichstein, M., Hollinger, D.Y., Richardson, A.D., Barr, A.G., Beckstein, C., Braswell, B.H., Churkina, G., Desai, A.R., Falge, E., 2007. Comprehensive comparison of gap-filling techniques for eddy covariance net carbon fluxes. Agric. For. Meteorol. 147 (3–4), 209–232. https://doi.org/10.1016/j.agrformet.2007.08.011.

Monteith, J.L., 1977. Climate and the efficiency of crop production in Britain. Philosophical Transactions of the Royal Society of London. B, Biological Sciences 281 (980), 277–294. https://doi.org/10.1098/rstb.1977.0140.

Nichol, C.J., Huemmrich, K.F., Black, T.A., Jarvis, P.G., Walthall, C.L., Grace, J., Hall, F.G., 2000. Remote sensing of photosynthetic-light-use efficiency of boreal forest. Agric. For. Meteorol. 101 (2–3), 131–142. https://doi.org/10.1016/S0168-1923(99)00167-7.

Ollinger, S.V., 2011. Sources of variability in canopy reflectance and the convergent properties of plants. New Phytol. 189 (2), 375–394. https://doi.org/10.1111/j.1469-8137.2010.03536.x.

Ollinger, S.V., Reich, P.B., Frolking, S., Lepine, L.C., Hollinger, D.Y., Richardson, A.D., 2013. Nitrogen cycling, forest canopy reflectance, and emergent properties of ecosystems. Proc. Natl. Acad. Sci. 110 (27), E2437. https://doi.org/10.1073/pnas.1304176110.

Ouimette, A.P., Ollinger, S.V., Richardson, A.D., Hollinger, D.Y., Keenan, T.F., Lepine, L.C., Vadeboncoeur, M.A., 2018. Carbon fluxes and interannual drivers in a temperate forest ecosystem assessed through comparison of top-down and bottom-up approaches. Agric. For. Meteorol. 256, 420–430. https://doi.org/10.1016/j.agrformet.2018.03.017.

Papale, D., Reichstein, M., Aubinet, M., Canfora, E., Bernhofer, C., Kutsch, W., Longdoz, B., Rambal, S., Valentini, R., Vesala, T., Yakir, D., 2006. Towards a standardized processing of Net Ecosystem Exchange measured with eddy covariance technique: algorithms and uncertainty estimation. Biogeosciences 3 (4), 571–583.

Peng, Y., Gitelson, A.A., 2011. Application of chlorophyll-related vegetation indices for remote estimation of maize productivity. Agric. For. Meteorol. 151 (9), 1267–1276. https://doi.org/10.1016/j.agrformet.2011.05.005.

Peng, Y., Gitelson, A.A., Keydan, G., Rundquist, D.C., Moses, W., 2011. Remote estimation of gross primary production in maize and support for a new paradigm based on total crop chlorophyll content. Remote Sens. Environ. 115 (4), 978–989. https://doi.org/10.1016/j.rse.2010.12.001.

Penuelas, J., Filella, I., Gamon, J.A., 1995. Assessment of photosynthetic radiation-use efficiency with spectral reflectance. New Phytol. 131 (3), 291–296. https://doi.org/10.1111/j.1469-8137.1995.tb03064.x.

Peñuelas, J., Garbulsky, M.F., Filella, I., 2011. Photochemical reflectance index (PRI) and remote sensing of plant CO_2 uptake. New Phytol. 191 (3), 596–599. https://doi.org/10.1111/j.1469-8137.2011.03791.x.

Piao, S., Sitch, S., Ciais, P., Friedlingstein, P., Peylin, P., Wang, X., Ahlström, A., Anav, A., Canadell, J.G., Cong, N., Huntingford, C., 2013. Evaluation of terrestrial carbon cycle models for their response to climate variability and to CO_2 trends. Glob. Chang. Biol. 19 (7), 2117–2132. https://doi.org/10.1111/gcb.12187.

Potter, C.S., Randerson, J.T., Field, C.B., Matson, P.A., Vitousek, P.M., Mooney, H.A., Klooster, S.A., 1993. Terrestrial ecosystem production: a process model based on global satellite and surface data. Glob. Biogeochem. Cycles 7 (4), 811–841. https://doi.org/10.1029/93GB02725.

Powell, T.L., Bracho, R., Li, J., Dore, S., Hinkle, C.R., Drake, B.G., 2006. Environmental controls over net ecosystem carbon exchange of scrub oak in central Florida. Agric. For. Meteorol. 141 (1), 19–34. https://doi.org/10.1016/j.agrformet.2006.09.002.

Raj, R., Hamm, N.A.S., Tol, C.V.D., Stein, A., 2016. Uncertainty analysis of gross primary production partitioned from net ecosystem exchange measurements. Biogeosciences 13 (5), 1409–1422. https://doi.org/10.5194/bg-13-1409-2016.

Rambal, S., Joffre, R., Ourcival, J.M., Cavender-Bares, J., Rocheteau, A., 2004. The growth respiration component in eddy CO_2 flux from a Quercus ilex Mediterranean forest. Glob. Chang. Biol. 10 (9), 1460–1469. https://doi.org/10.1111/j.1365-2486.2004.00819.x.

Reich, P.B., 2012. Key canopy traits drive forest productivity. Proc. R. Soc. Lond. B Biol. Sci. https://doi.org/10.1098/rspb.2011.2270. p.rspb20112270.

Reichstein, M., Falge, E., Baldocchi, D., Papale, D., Aubinet, M., Berbigier, P., Bernhofer, C., Buchmann, N., Gilmanov, T., Granier, A., Grünwald, T., 2005. On the separation of net ecosystem exchange into assimilation and ecosystem respiration: review and improved algorithm. Glob. Chang. Biol. 11 (9), 1424–1439. https://doi.org/10.1111/j.1365-2486.2005.001002.x.

Rice, A.H., Pyle, E.H., Saleska, S.R., Hutyra, L., Palace, M., Keller, M., De Camargo, P.B., Portilho, K., Marques, D.F., Wofsy, S.C., 2004. Carbon balance and vegetation dynamics in an old-growth Amazonian forest. Ecol. Appl. 14 (sp4), 55–71. https://doi.org/10.1890/02-6006.

Rouse, J.W., Haas, R.H., Schell, J.A., Deering, D.W., 1973. Monitoring vegetation systems in the Great Plains with ERTS. In: Proc. Third Earth Resources Technology Satellite-1 Symposium, Goddard Space Flight Center, NASA SP-351. Science and Technical Information Office, NASA, Washington, DC, pp. 309–317.

Running, S.W., Zhao, M., 2015. User's Guide Daily GPP and Annual NPP (MOD17A2/A3) Products, NASA Earth Observing System MODIS Land Algorithm, Version 3.0. https://www.ntsg.umt.edu/files/modis/MOD17UsersGuide2015_v3.pdf, Accessed date: 12 April 2018.

Running, S.W., Nemani, R.R., Heinsch, F.A., Zhao, M., Reeves, M., Hashimoto, H., 2004. A continuous satellite-derived measure of global terrestrial primary production. AIBS Bull. 54 (6), 547–560. https://doi.org/10.1641/0006-3568(2004)054[0547:ACSMOG]2.0.CO;2.

Russell, G., Jarvis, P.G., Monteith, J.L., 1989. Absorption of radiation by canopies and stand growth. In: Russell, G., Marshall, B., Jarvis, P.G. (Eds.), Plant Canopies: Their Growth, Form and Function. Cambridge University Press, Cambridge, pp. 21–40.

Savitzky, A., Golay, M.J., 1964. Smoothing and differentiation of data by simplified least squares procedures. Anal. Chem. 36 (8), 1627–1639. https://doi.org/10.1021/ac60214a047.

Schaefer, K., Schwalm, C.R., Williams, C., Arain, M.A., Barr, A., Chen, J.M., Davis, K.J., Dimitrov, D., Hilton, T.W., Hollinger, D.Y., Humphreys, E., 2012. A model-data comparison of gross primary productivity: results from the North American Carbon Program site synthesis. Journal of Geophysical Research: Biogeosciences 117 (G3). https://doi.org/10.1029/2012JG001960.

Schimel, D., Pavlick, R., Fisher, J.B., Asner, G.P., Saatchi, S., Townsend, P., Miller, C., Frankenberg, C., Hibbard, K., Cox, P., 2015. Observing terrestrial ecosystems and the

carbon cycle from space. Glob. Chang. Biol. 21 (5), 1762–1776. https://doi.org/10.1111/gcb.12822.

Schmidt, M.W., Torn, M.S., Abiven, S., Dittmar, T., Guggenberger, G., Janssens, I.A., Kleber, M., Kögel-Knabner, I., Lehmann, J., Manning, D.A., Nannipieri, P., 2011. Persistence of soil organic matter as an ecosystem property. Nature 478 (7367), 49. https://doi.org/10.1038/nature10386.

Schmidt, A., Hanson, C., Chan, W.S., Law, B.E., 2012. Empirical assessment of uncertainties of meteorological parameters and turbulent fluxes in the AmeriFlux network. Journal of Geophysical Research: Biogeosciences 117 (G4). https://doi.org/10.1029/2012JG002100.

Scott, R.L., Jenerette, G.D., Potts, D.L., Huxman, T.E., 2009. Effects of seasonal drought on net carbon dioxide exchange from a woody-plant-encroached semiarid grassland. Journal of Geophysical Research: Biogeosciences 114 (G4). https://doi.org/10.1029/2008JG000900.

Serbin, S.P., Dillaway, D.N., Kruger, E.L., Townsend, P.A., 2011. Leaf optical properties reflect variation in photosynthetic metabolism and its sensitivity to temperature. J. Exp. Bot. 63 (1), 489–502. https://doi.org/10.1093/jxb/err294.

Serbin, S.P., Singh, A., Desai, A.R., Dubois, S.G., Jablonski, A.D., Kingdon, C.C., Kruger, E.L., Townsend, P.A., 2015. Remotely estimating photosynthetic capacity, and its response to temperature, in vegetation canopies using imaging spectroscopy. Remote Sens. Environ. 167, 78–87. https://doi.org/10.1016/j.rse.2015.05.024.

Sommer, R., de Abreu Sá, T.D., Vielhauer, K., de Araújo, A.C., Fölster, H., Vlek, P.L., 2002. Transpiration and canopy conductance of secondary vegetation in the eastern Amazon. Agric. For. Meteorol. 112 (2), 103–121. https://doi.org/10.1016/S0168-1923(02)00044-8.

Suyker, A.E., Verma, S.B., Burba, G.G., Arkebauer, T.J., Walters, D.T., Hubbard, K.G., 2004. Growing season carbon dioxide exchange in irrigated and rainfed maize. Agric. For. Meteorol. 124 (1–2), 1–13. https://doi.org/10.1016/j.agrformet.2004.01.011.

Suyker, A.E., Verma, S.B., Burba, G.G., Arkebauer, T.J., 2005. Gross primary production and ecosystem respiration of irrigated maize and irrigated soybean during a growing season. Agric. For. Meteorol. 131 (3–4), 180–190. https://doi.org/10.1016/j.agrformet.2005.05.007.

Tucker, C.J., 1979. Red and photographic infrared linear combinations for monitoring vegetation. Remote Sens. Environ. 8 (2), 127–150. https://doi.org/10.1016/0034-4257(79)90013-0.

Turner, D.P., Urbanski, S., Bremer, D., Wofsy, S.C., Meyers, T., Gower, S.T., Gregory, M., 2003. A cross-biome comparison of daily light use efficiency for gross primary production. Glob. Chang. Biol. 9 (3), 383–395. https://doi.org/10.1046/j.1365-2486.2003.00573.x.

Urbanski, S., Barford, C., Wofsy, S., Kucharik, C., Pyle, E., Budney, J., McKain, K., Fitzjarrald, D., Czikowsky, M., Munger, J.W., 2007. Factors controlling CO_2 exchange on timescales from hourly to decadal at Harvard Forest. Journal of Geophysical Research: Biogeosciences (G2), 112. https://doi.org/10.1029/2006JG000293.

Verma, S.B., Dobermann, A., Cassman, K.G., Walters, D.T., Knops, J.M., Arkebauer, T.J., Suyker, A.E., Burba, G.G., Amos, B., Yang, H., Ginting, D., 2005. Annual carbon dioxide exchange in irrigated and rainfed maize-based agroecosystems. Agric. For. Meteorol. 131 (1–2), 77–96. https://doi.org/10.1016/j.agrformet.2005.05.003.

Vourlitis, G.L., Priante Filho, N., Hayashi, M., Nogueira, J.D.S., Raiter, F., Hoegel, W., Campelo Jr., J.H., 2004. Effects of meteorological variations on the CO_2 exchange of a Brazilian transitional tropical forest. Ecol. Appl. 14 (sp4), 89–100. https://doi.org/10.1890/01-6005.

Wold, S., Sjöström, M., Eriksson, L., 2001. PLS-regression: a basic tool of chemometrics. Chemom. Intell. Lab. Syst. 58 (2), 109–130. https://doi.org/10.1016/S0169-7439(01)00155-1.

Wong, C., Gamon, J.A., 2015. The photochemical reflectance index provides an optical indicator of spring photosynthetic activation in evergreen conifers. New Phytol. 206 (1), 196–208. https://doi.org/10.1111/nph.13251.

Xu, B., Park, T., Yan, K., Chen, C., Zeng, Y., Song, W., Yin, G., Li, J., Liu, Q., Knyazikhin, Y., Myneni, R.B., 2018. Analysis of global LAI/FPAR products from VIIRS and MODIS sensors for spatio-temporal consistency and uncertainty from 2012–2016. Forests 9 (2), 73–94. https://doi.org/10.3390/f9020073.